Etching induced formation of interfacial FeMn in IrMn/CoFe bilayers

Etching induced formation of interfacial FeMn in IrMn/CoFe bilayers

Etching induced formation of interfacial FeMn in IrMn/CoFe bilayers

D. O'Donnell,[1] S. Hassan,[1] Y. Du,[1] N. Gauquelin,[2] D. Krishnan,[2]
J. Verbeeck,[2] R. Fan,[3] P. Steadman,[3] P. Bencok,[3] and A. N. Dobrynin[1,*]

[1]*Seagate Technology, 1 Disc Drive, Derry, BT48 0BF, Northern Ireland, UK*
[2]*EMAT, Universiteit Antwerpen, Gronenborgerlaan 171, 2020, Antwerpen, Belgium*
[3]*Diamond Light Source, Harwell Science and Innovation Campus, Didcot, OX11 0DE, Oxon, UK*

Effect of ion etching on exchange bias in $IrMn_3/Co_{70}Fe_{30}$ bilayers is investigated. In spite of the reduction of saturation magnetization caused by embedding of Ir from the capping layer into the $Co_{70}Fe_{30}$ layer during the etching process, the exchange bias in samples with the same thickness of the $Co_{70}Fe_{30}$ layer is reducing in proportion to the etching power. XMCD measurements revealed the emergence of an uncompensated Mn magnetization after etching, which is antiferromagnetically coupled to the ferromagnetic layer. This suggests etching induced formation of small interfacial FeMn regions which leads to the decrease of effective exchange coupling between ferromagnetic and antiferromagnetic layers.

Exchange bias effect appears in ferromagnetic (FM) - antiferromagnetic (AFM) nanoscale systems when the AFM interfacial spin structure is set in a certain direction either by deposition / annealing in magnetic field or by field cooling through the AFM's Néel temperature [1, 2]. This leads to developing of unidirectional anisotropy, when it is easier to reverse the FM part magnetization in the direction of the deposition / annealing / cooling field than in the opposite field direction, i.e., a horizontal shift of the magnetic hysteresil loop develops. Technologicaly unidirectional unisotropy is widely used for pinning FM layers in required directions in hard disk drive (HDD) read / write heads [3–5] and magnetic random access memory (MRAM) [6, 7]. IrMn is the most technologically relevant AFM material due to its range of blocking temperatures allowing to set the AFM by annealing in field without affecting the rest of the stack layers [8–11]. The pinning strength, which is determined by the interfacial FM / AFM exchange energy, is the most critical parameter, which in particular defines the device stability and possibility of reversal of the pinned FM layers by operational magnetic fields or spin transfer torques (STT) [12, 13]. In this work we focus on the effect of ion etching of the FM layer on exchange bias. Such etching can be a part of magnetic tunnel junction (MTJ) and MRAM stack definition, and it is important to understand its effects on the exchange coupling at the FM/AFM interface in particlular with a view to controlling the pinning field strength.

The samples were prepared by DC magnetron sputtering in Anelva C7100 deposition system at the base pressure of 10^{-9} mbar. First a 1.5 nm Ta / 1.8 nm Ru buffer layer was deposited on a thermally oxidized 200 mm Si/SiO_2 wafers, following by a 7 nm thick $IrMn_3$, which was deposited at 350°C. For one (reference) sample a 2.5 nm thick $Co_{70}Fe_{30}$ was deposited at 250°C on top of the $IrMn_3$ layer, and capped with a 2 nm thick MgO layer. For other samples a 5 nm $Co_{70}Fe_{30}$ layer was deposited 250°C first, capped with 2 nm of Ir. These samples were then transferred to the etching chamber, where they were etched back to 2.5 nm by Ar^+ ions at 50 ccm Ar gas flow and at powers of 50W, 100W, 250W, and 300W. The etching rate for the $Co_{70}Fe_{30}$ 5 nm / Ir 2 nm bilayer was calibrated for different powers to target the 2.5 nm thick $Co_{70}Fe_{30}$ layers. After etching the samples were capped with 2 nm thick MgO layers. After the deposition the wafers were annealed at 300°C in the applied magnetic field of 5 T, in order to induce the easy axis of exchange anisotropy along the applied field direction.

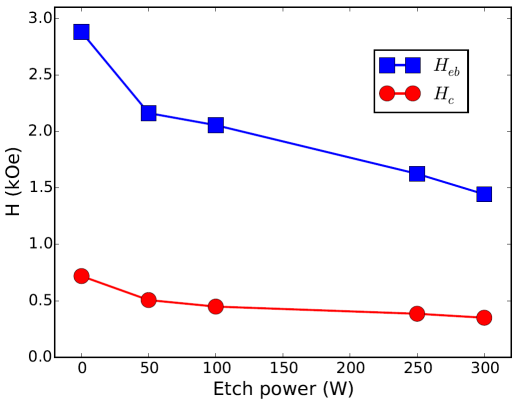

FIG. 1: Coercive field (H_c) and exchange bias field (H_{eb}) of $IrMn_3/Co_{70}Fe_{30}$ samples as a function of the etching power.

X-ray diffraction (XRD) was performed on all five samples using Cu K-α radiation in θ-2θ geometry. Cubic structures for both $Co_{70}Fe_{30}$ and $IrMn_3$ were confirmed with the lattice parameters of 2.88 $\AA$ for $Co_{70}Fe_{30}$ and 3.77 $\AA$ for $IrMn_3$ respectively. No significant XRD peak shifts as a function of the etching power were observed.

*Electronic address: alexey.dobrynin@seagate.com

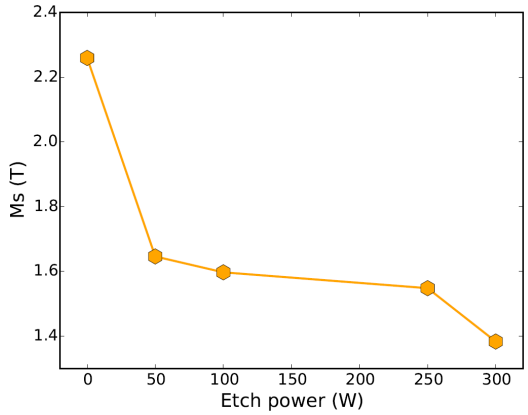

FIG. 2: Dependence of the $Co_{70}Fe_{30}$ layer's saturation magnetization on the etching power.

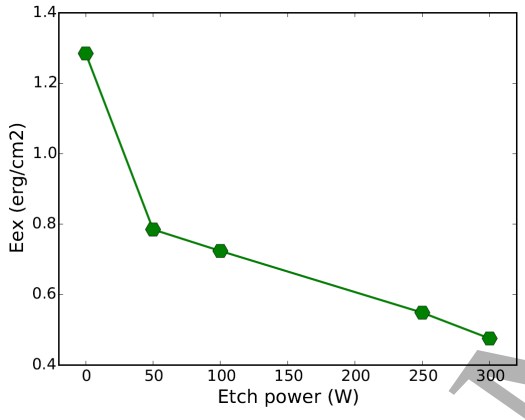

FIG. 3: Dependence of the interfacial exchange energy density between $Co_{70}Fe_{30}$ and $IrMn_3$ layers (b) on the etching power.

$IrMn_3$ has strong (111) texture, with only (111) and (222) peaks present. This also confirms absence of the ordered $L1_2$ $IrMn_3$ phase, as although disordered γ and orderd $L1_2$ $IrMn_3$ phases have very close lattice paramters, all allowed reflections for disordered γ $IrMn_3$ have either all Miller indicies hkl even or all hkl odd, while for the ordered phase combinatons of odd and even h,k and l are allowed [14]. The thicknesses of the $Co_{70}Fe_{30}$ layers were measured by X-ray fluorescence (XRF), and they were 2.5 nm, 2.8 nm, 2.8 nm, 2.7 nm, 3.0 nm for samples etched at 0W, 50W, 100W, 250W, and 300W correspondingly, with the relative error of the measurements being 1 %.

Magnetization measurements were performed in a BH looper at room temperature. Fig. 1 shows dependence of obtained coercivity and exchange bias fields for samples etched at different powers. It can be seen that both H_c and H_{eb} decrease progressively with the etching power, with 2 fold drop in the H_{eb} value from 2881 Oe to 1444 Oe between the unetched and etched at 300 W samples. Fig. 2 (a) shows the dependence

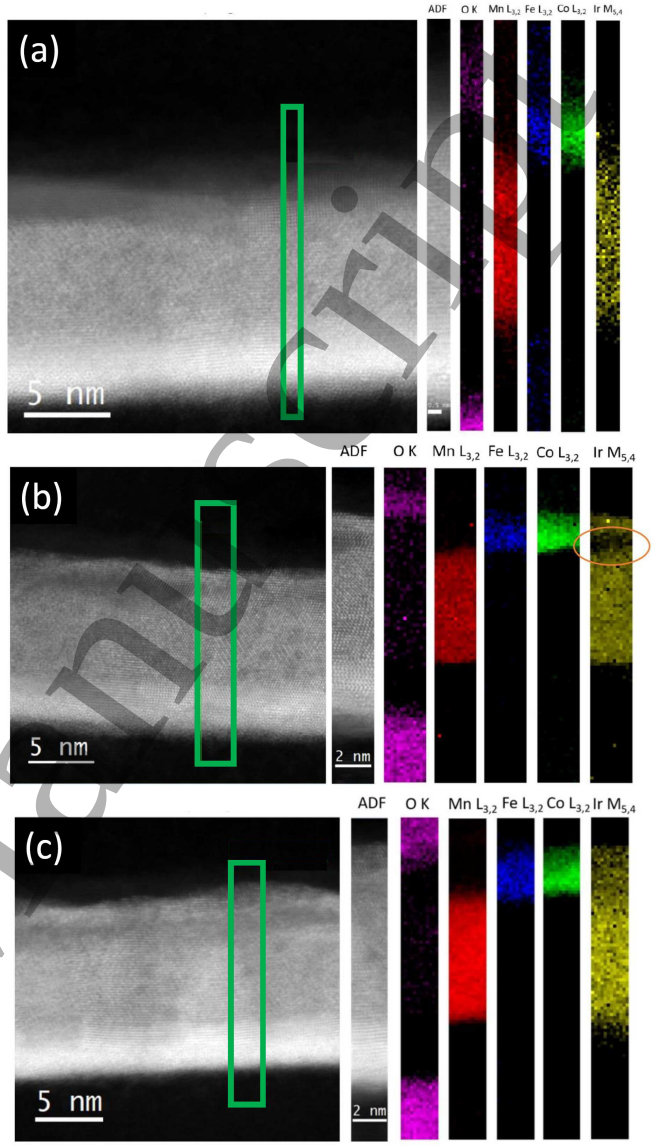

FIG. 4: Cross section HAADF-STEM and EELS imaging of samples etched at 0W (a), 100W (b) and 300W (c). Green rectangles on the STEM images (left panel) designate the areas on which EELS analysis has been performed. From EELS elemental mapping it can be seen that $Co_{70}Fe_{30}$ layer is being contaminated by Ir as etching power increases. At a lower etching power of 100 W Ir contamination is limited to the top part of the $Co_{70}Fe_{30}$ layer (b). At the etching power of 300 W embedded Ir can be seen throughout the $Co_{70}Fe_{30}$ layer (c).

of the saturation magnetization M_s as a function of the etching power, also showing significant decrease of M_s after etching, from 22.6 kG to 13.8 kG. The corresponding exchange bias energy density, obtained from the expression $E_{ex} = H_{eb}M_s t_{FM}$, where t_{FM} is the thickness of the FM layer, is shown in Fig. 2 (b). E_{ex} reduction from 1.29 erg/cm^2 for the not etched sample to 0.48 erg/cm^2 for sample etched at 300 W is observed.

High Angle Annular Dark Field Scanning Transmission Electron Microscopy (HAADF-STEM) and electron energy loss spectroscopy (EELS) were performed using FEI Titan^3 microscope. Cross-sections of the samples were prepared in inert atmosphere using a method described elsewhere [15, 16]. EELS mapping was performed at the following absorption edges: O (K edge), Mn ($L_{2,3}$ edges), Fe ($L_{2,3}$ edges), Co ($L_{2,3}$ edges), Ir ($M_{4,5}$ edges). On the left hand side of Fig. 4 HAADF-STEM images of samples etched at 0W (unetched), 100W, and 300W are presented. On the right hand side of the same figure EELS elemental maps obtained from the regions contained in the rectangular areas shown on the left are displayed. A clear contamination, resulting from etching of the Ir capping layer, is observed for samples etched at 100W (Fig. 4 (b)) and at 300W (Fig. 4 (c)). The diffusion length of the Ir from the surface of the CoFe layer towards the CoFe/$IrMn_3$ interface is increasing with etching power. For the sample etched at 300 W the Ir contamination is maximal, propagating all the way through the CoFe layer. This means that the Ir layer, which is used as a temporary pre-etching capping layer, is being embedded into the CoFe layer, thus reducing its M_s, as it was evident from magnetization measurements.

Soft X-ray magnetic circular dichroism measurements (XMCD) were performed at the I10 beamline, Diamond Light Source, on the high field magnet absorption endstation. Right and left circular polarisation of the incident X-ray beam was provided by I10's versatile helical insertion devices [17], and energy was selected by a plane grating monochromator (PGM) [18, 19] using a gold coated grating with 400 lines per mm density, providing resolving power ($E/\Delta E$) of better than 7000. Fast energy scans [20] were used with insertion device magnets and PGM's grating being moved simulteneously. This allowed to reduce time of one X-ray absorption (XAS) spectrum collection over $L_{2,3}$ edges of Co, Fe, or Mn (usually a 50 eV range) to less than 2 minutes, thus minimizing effects of beam instability on the XAS spectra.

The samples were placed inside a split pair superconducing magnet, and the field of 20 kOe was applied along the X-ray beam direction. The planes of the samples were positioned at an angle of 10° with respect to the incident beam. Measurements were performed at the temperature of 290 K. Total fluorescence yield (TFY) was detected using a photodiode. XAS spectra were measured first with right circular polarisation of the incident X-ray beam, followed by the same scan taken with left circular polarisation of the beam, and the XMCD signal was obtained by subtracting the latter from the former. Fig. 5 shows XAS and XMCD spectra for the unetched sample, measured with TFY. Negative XMCD signal at the L_3 edges of Fe and Co indicate their parallel alignment along the applied field, while XMCD signal at the Mn edges for this sample is zero, meaning zero net magnetization of Mn for the unetched sample. XAS spectra

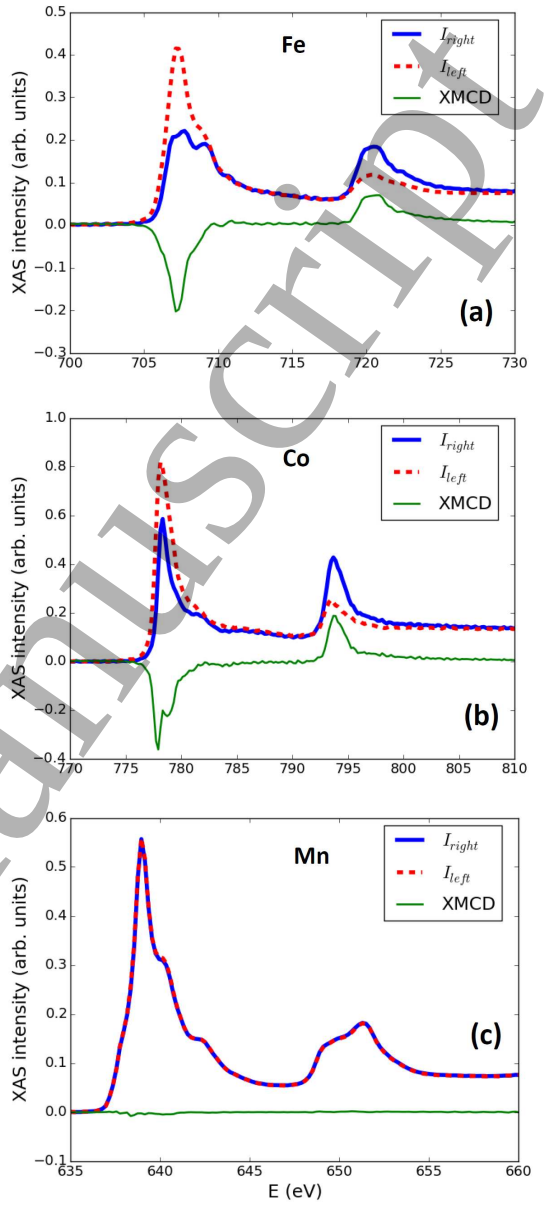

FIG. 5: XAS spectra of the unetched sample measured across Fe (a), Co (b), and Mn (c) $L_{2,3}$ absorption edges at grazing incidence with rigth and lefct circularly polarised soft X-ray radiation at the applied magnetic field of 2 T applied along the beam direction. Total fluorescence yield was used to detect the signal. Plotted XMCD signal is the difference between XAS specra measured with right and left circular polarisations.

across the Mn L_3 edge for samples etched at 0W, 50W, and 250W are shown in Fig. 6. Uncompensated Mn magnetization emerges after etching, as evident from Fig. 6 (b) and (c). Although we can't quantify this uncompensated magnetization, it can be seen that the XMCD signal for the sample etched at 50W is smaller than that for sample etched at 250W, which indicates larger amount of uncompensated Mn magnetization for the latter sample. The positive sign of the Mn XMCD signal at the L_3 ab-

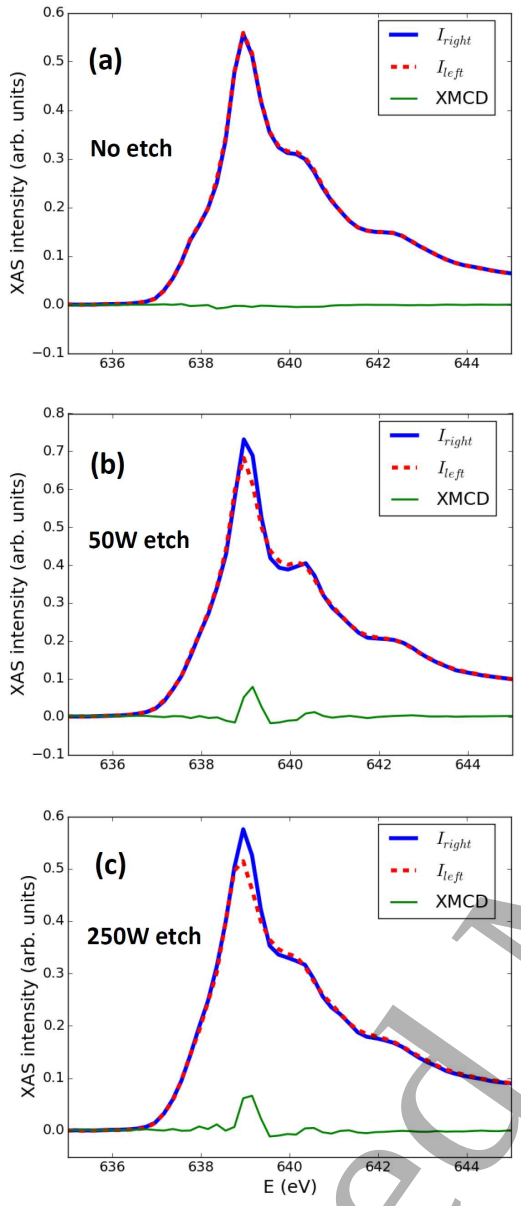

FIG. 6: XAS spectra measured at the Mn L_3 absorption edge at grazing incidence with rigth and lefct circularly polarised soft X-ray radiation at the applied magnetic field of 20 kG applied along the beam direction. (a) - unetched sample; (b) - sample etched at 50W; (c) - sample etched at 250W. While zero for the etched sample (a), a positive XMCD signal develops post-etching, as evident from (b) and (c). The positive sign of the XMCD signal at the L_3 edge, as opposed to the negative sign at the L_3 edge for Co and Fe suggests antiparallel orientation of Mn magnetization to that of Fe and Co.

sorption edge, as opposed to the negative XMCD sign at the L_3 edge for Co and Fe implies antiparallel alignment of Mn uncompensated moment to Co and Fe magnetic moments.

It is known that interfacial exchange coupling between Co and Mn is ferromagnetic [21, 22], while that between Fe and Mn is antiferromagnetic [23–26]. Tsunoda, Takahashi et al. performed systematic XMCD study of $Ni_{100-x}Co_x$, $Co_{100-x}Fe_x$, and $Fe_{100-x}Ni_x$ exchange coupled to IrMn [27, 28]. For $Co_{100-x}Fe_x$ alloy they observed transition from ferromagnetic to antiferromagnetic coupling of Mn uncompensated moments to the FM film for $x > 80\%$. Thus we can come up with two possible interpretations of the observed behavior. The first one is a formation of Fe rich regions due to Co:Fe segregation at the interface. This is consistent with the reduction of the net interfacial exchange energy after etching, as the Fe rich regions coupled to Mn provide exchange bias in the opposite direction from that provided by the regions rich in Co, while Co and Fe rich interfacial regions remain ferromagnetically coupled to each other. The second interpretation comes from the fact that it is impossible to exclude some interdiffusion at the interface, although it wasn't observed in cross-sectional EELS measurements. This can be understood as the spatial resolution in projection is limited due to the interfaces not being atomically flat and the ability of EELS to detect low concentration of elements is hampered by the limited signal to noise ratio. Structural roughness of the interface is mainly due to the granular structure of IrMn, which has a mean grain size of about 6-7 nm [10], which defines the in-plane roughness length. This large scale interfacial roughness, unlike the atomistic roughness of the interface, is not affected by etching. As etching induced FeMn formation is evident from XMCD measurements, we can envisage two ways of interfacial interdiffusion. In the first case Co from the CoFe layer diffuses into the IrMn layer, and Mn from IrMn diffuses into the CoFe layer, forming small FeMn clusters ferromagnetically exchange coupled to the rest of the CoFe film. Diffusion of Co into the IrMn layer supresses the AFM ordering of the later, creating exchange decoupled regions, which in turn leads to the decrease of the exchange bias field. In the second case there is no diffusion from the IrMn layer, but Fe from the CoFe layer diffuses into the IrMn layer, again forming small FeMn clusters, and reducing overall exchange coupling due to altering of the AFM order at the interfacial regions where such FeMn clustering occurs.

In summary we investigated the effects of Ar^+ ion etching on exchange bias in $IrMn_3$ / $Co_{70}Fe_{30}$ bilayers. The $Co_{70}Fe_{30}$ layers were prepared by depositing 5 nm of $Co_{70}Fe_{30}$, capping it with 2nm of Ir, and then etching back to 2.5nm of $Co_{70}Fe_{30}$. Significant drop in the exchange bias field was observed for the etched samples, in spite of the reduced M_s in these samples as compared to the reference unetched sample. All the samples were annealed in identical conditions, so effects of thermal diffusion on exchange bias [29], if they were present, can not account for the observed differences in magnetic properties. EELS measurements revealed significant fraction of embedded Ir in the CoFe layer, resulting from the temporary Ir cap deposited on top of the CoFe layer before etching. The distribution of embedded Ir in the etched

CoFe layers is inhomogeneous, with most of the Ir being close to the surface of the film. For the samples etched at low powers almost no Ir from the cap propagates down to the IrMn / CoFe interface, while for the highest etching power some of Ir from the cap reaches the interface. However no crystal structure modifications was observed neither by XRD nor by TEM, suggesting that there is no alloying between Ir and CoFe. This implies that the effect of embedding of Ir on magnetic properties of the system is purely in the decrease of M_s of the CoFe layer. It is important to stress that such M_s decrease would lead to an increase of the exchange bias field should the interfacial exchange energy density remain constant. The opposite trend of H_{eb} vs M_s implies significant decrease of the interfacial exchange energy density after etching. Soft X-ray XMCD measurements at the $L_{2,3}$ absorption edges revealed emergence of uncompensated Mn magnetic moments, which are antiparallel to the magnetization of the CoFe layer. This implies formation of interfacial FeMn regions after etching, which results in reduction of the effective interfacial exchange coupling energy between FM and AFM layers. There are two possible casues of such interfacial FeMn formation: (i) segregation of Co and Fe at the interface, or (ii) interdiffuion of Co into IrMn and Mn into CoFe or Fe into FeMn, leading to formation of small FeMn clusters. The mechanisms of exchange bias reduction in the two cases are different: in the first case CoFe regions rich in Fe provide exchange bias in the opposite direction to that provided by the CoFe regions rich in Co, thus reducing the resulting exchange bias field; in the second case interfacial FeMn cluster formation alters interfacial AFM structure, and reduces net exchange coupling energy. The mechanism for such local composition changes at the interface must be knock on energy transfer from Ar^+ ions bombarding the top surface of the CoFe film. We believe that our results improve fundamental understanding of exchange bias effect in CoFe / IrMn systems, and they are of particular technological importance, providing a way to control the pinning strength in CoFe / IrMn bilayers by changing the etching power of the FM layer.

[1] W. H. Meiklejohn and C. P. Bean, Phys. Rev. **102**, 1413 (1956).
[2] J. Nogués, J. Sort, V. Langlais, V. Skumryev, S. Suriach, J. Muoz, and M. Bar, Physics Reports **422**, 65 (2005).
[3] J. R. Childress and R. E. Fontana, Comptes Rendus Physique **6**, 997 (2005).
[4] O. G. Heinonen, E. W. Singleton, B. W. Karr, Z. Gao, H. S. Cho, and Y. Chen, IEEE Transactions on Magnetics **44**, 2465 (2008).
[5] J. C. S. Kools, IEEE Transactions on Magnetics **32**, 3165 (1996).
[6] S. S. P. Parkin, K. P. Roche, M. G. Samant, P. M. Rice, R. B. Beyers, R. E. Scheuerlein, E. J. O'Sullivan, S. L. Brown, J. Bucchigano, D. W. Abraham, et al., Journal of Applied Physics **85**, 5828 (1999).
[7] S. Tehrani, B. Engel, J. M. Slaughter, E. Chen, M. DeHerrera, M. Durlam, P. Naji, R. Whig, J. Janesky, and J. Calder, IEEE Transactions on Magnetics **36**, 2752 (2000).
[8] G. Anderson, Y. Huai, and L. Miloslawsky, Journal of Applied Physics **87**, 6989 (2000).
[9] L. E. Fernandez-Outon, K. O'Grady, S. Oh, M. Zhou, and M. Pakala, IEEE Transactions on Magnetics **44**, 2824 (2008).
[10] G. Vallejo-Fernandez, N. P. Aley, L. E. Fernandez-Outon, and K. O'Grady, Journal of Applied Physics **104**, 033906 (2008).
[11] V. Baltz, Applied Physics Letters **102**, 062410 (2013).
[12] J. Katine and E. E. Fullerton, Journal of Magnetism and Magnetic Materials **320**, 1217 (2008).
[13] D. Apalkov, A. Khvalkovskiy, S. Watts, V. Nikitin, X. Tang, D. Lottis, K. Moon, X. Luo, E. Chen, A. Ong, et al., J. Emerg. Technol. Comput. Syst. **9**, 13:1 (2013).
[14] A. Kohn, A. Kovacs, R. Fan, G. J. McIntyre, R. C. C. Ward, and J. P. Goff, Scientific Reports **3**, 2412 (2013).
[15] B. Conings, J. Drijkoningen, N. Gauquelin, A. Babayigit, J. D'Haen, L. D'Olieslaeger, A. Ethirajan, J. Verbeeck, J. Manca, E. Mosconi, et al., Advanced Energy Materials **5**, 1500477 (2015).
[16] E. Grieten, O. Schalm, P. Tack, S. Bauters, P. Storme, N. Gauquelin, J. Caen, A. Patelli, L. Vincze, and D. Schryvers, Journal of Cultural Heritage **28**, 56 (2017).
[17] E. C. Longhi, P. Bencok, A. Dobrynin, E. C. M. Rial, A. Rose, P. Steadman, C. Thompson, A. Thomson, and H. Wang, Journal of Physics: Conference Series **425**, 032011 (2013).
[18] F. Senf, K. J. S. Sawhney, R. Follath, M. Scheer, F. Schäfers, J. Bahrdt, A. Gaupp, and W. Gudat, Journal of Synchrotron Radiation **5**, 747 (1998).
[19] R. Follath, F. Senf, and W. Gudat, Journal of Synchrotron Radiation **5**, 769 (1998).
[20] J. Krempasky, U. Flechsig, T. Korhonen, D. Zimoch, C. Quitmann, and F. Nolting, AIP Conference Proceedings **1234**, 705 (2010).
[21] W. L. O'Brien and B. P. Tonner, Phys. Rev. B **50**, 2963 (1994).
[22] Y. Yonamoto, T. Yokoyama, K. Amemiya, D. Matsumura, and T. Ohta, Phys. Rev. B **63**, 214406 (2001).
[23] C. Roth, T. Kleemann, F. U. Hillebrecht, and E. Kisker, Phys. Rev. B **52**, R15691 (1995).
[24] O. Rader, W. Gudat, D. Schmitz, C. Carbone, and W. Eberhardt, Phys. Rev. B **56**, 5053 (1997).
[25] J. Dresselhaus, D. Spanke, F. U. Hillebrecht, E. Kisker, G. van der Laan, J. B. Goedkoop, and N. B. Brookes, Phys. Rev. B **56**, 5461 (1997).
[26] S. Brück, S. Macke, E. Goering, X. Ji, Q. Zhan, and K. M. Krishnan, Phys. Rev. B **81**, 134414 (2010).
[27] M. Tsunoda, H. Takahashi, T. Nakamura, C. Mitsumata, S. Isogami, and M. Takahashi, Applied Physics Letters **97**, 072501 (2010).
[28] H. Takahashi, Y. Kota, M. Tsunoda, T. Nakamura, K. Kodama, A. Sakuma, and M. Takahashi, Journal of Applied Physics **110**, 123920 (2011).
[29] F. Letellier, L. Lechevallier, R. Lard, J.-M. Le Breton,

K. Akmaldinov, S. Auffret, B. Dieny, and V. Baltz, Journal of Applied Physics **116**, 203906 (2014).